Electron Transfer Mediating Properties of Hydrocarbons as a Function of Chain Length: A Differential Scanning Conductive Tip Atomic Force Microscopy Investigation

Denis Scaini,[†,‡] Matteo Castronovo,[‡,§] Loredana Casalis,[†] and Giacinto Scoles[†,§,⊥,*]

[†]SISSA/ETTRA NanoInnovation Laboratory, Sincrotrone Trieste, S.S.14 Km 163.5, 34012 Basovizza, Trieste, Italy, [‡]Physics Department, University of Trieste, P. Europa 1, 34127 Trieste, Italy, [§]International School for Advanced Studies, Via Beirut 4, 34100 Trieste, Italy, and [⊥]Chemistry Department, University of Princeton, Princeton, New Jersey 08544

ABSTRACT The development of novel molecular and biomolecular devices relies on the understanding of charge transport across molecule-substrate interfaces. However, different strategies adopted so far for fabricating and studying transport through metal—molecule—metal junctions yield values for the transport coefficients that differ by up to orders of magnitude even for the same junction. Conductive tip atomic force microscopy (CT-AFM) allows for the simultaneous measurement of transport and morphological properties of molecular assemblies, but absolute transport measurements depend on the nature of the AFM tip—molecule contact. In this work we present a differential approach to the study of metal—molecule—metal junctions based on the combination of AFM-driven nanolithography and CT-AFM. We nanograft patches of alkanethiol molecules in a self-assembled monolayer of alkanethiol molecules of different chain length and measure by CT-AFM the morphology and the transport properties of the nanopatches and of the reference layer. The method allows for the determination of the differential resistance between the two molecular layers and is thus independent of environmental factors. The validity of this approach is demonstrated by measuring the tunneling decay constant of alkanethiols as a function of their length.

KEYWORDS: nanolithography · atomic force microscopy · nanografting · alkanethiols · differential measurements · transport properties · tunneling

Understanding charge transport at the molecular level is of crucial importance for developing molecular assemblies with uncommon properties for novel applications, such as molecular electronic devices and sensors.[1–5] Precise measurements of the charge transport and tunneling at the contacts and through the molecules are likely to provide crucial insight into the electronic couplings within and between molecules and with the interface.[6] From a more general point of view, such studies aim at expanding our fundamental understanding of molecular electronics: a central issue in biophysics and biochemistry.

Metal—molecule—metal junctions (M-m-M) have been extensively studied in the past years in order to understand the factors influencing the transport of charges through or across different molecules. Systems ranging from a single molecule contacted by two metal electrodes to self-assembled monolayers (SAMs) sandwiched between two contacts have been investigated by using an array of different techniques. Unfortunately there is a wide spectrum of factors influencing the electron transfer behavior in these systems which is responsible for the presence of large inconsistencies in the literature. Values spreading over 3 orders of magnitude are easily found for the same molecule.[7]

Strategies for fabricating M-m-M junctions include assembling of molecules into metal-capped nanopores[8,9] or between a semiconductor surface and a mercury drop.[10,11] Also, mechanically controlled break junctions[12–14] and nanofabricated electrodes[15] or crossed wires[16] have been used. Of particular interest is the use of the metallic tip of a scanning probe microscope to form and characterize M-m-M junctions.[17–20] Scanning tunneling microscopy (STM) and conductive tip atomic force microscopy (CT-AFM) are ideally suited to make local measurements of electron transfer through organic thin films. In both cases, in fact, it is possible to record simultaneously electron transport details (in both instruments the tip interacts with the sample *via* electron tunneling) and the spatial characterization of the molecules. The major distinction between the two

See the accompanying Perspective by Bumm on p 403.

*Address correspondence to scoles@sissa.it.

Received for review November 2, 2007 and accepted January 30, 2008.

Published online February 12, 2008.
10.1021/nn700342p CCC: $40.75

techniques concerns the feedback signal used. In the STM case, the current itself is used as feedback signal while in CT-AFM the optical feedback is enforced even during current measurements. The advantage of this second solution is the possibility to use high-gain, low-noise, and therefore slow, amplifiers even with highly corrugated samples. This is more difficult with STM because the amplifier has to be fast enough to allow for the feedback to follow the sample morphology. This limits the current to about 10 pA or higher for routine measurements. Another point to remember when using an STM is the change in tip–surface distance (or in electrical parameters) that happens when the probe moves above differently conductive molecules.[18]

A common characteristic of the almost totality of approaches evolved so far is the fact that they rely on *absolute* transport measurements with the consequence that the values obtained are strongly affected by the experimental boundary conditions. Molecular dimensions (and so, indirectly, the distance between the two electrodes), molecular HOMO–LUMO energy gaps, molecular ionization potentials, metal work functions, molecule−substrate bonding and functional group architectures, contact properties (*i.e.*, the number of molecules involved) all have a strong impact on the transport characteristics.[21−24] Moreover, to these factors, other factors that influence the measurements have to be added, such as substrate roughness, tip chemistry, the possible presence of solvent or water meniscus, extended tip usage, and contact dimension, which is related to the radius of the tip in the case of AFM studies. It follows, that it is next to impossible to compare not only current values coming from different techniques but frequently also values coming from the same experimental run. In fact, for example, it is hard to verify whether, from the beginning to the end of an experiment, the tip always maintains the same conditions.

To overcome these problems a differential approach has to be considered. In fact, measuring simultaneously at least two different monolayers, self-assembled side-by-side on the same surface, eliminates most of the above-mentioned difficulties. When the ratio between the values of the current through the different molecules is considered, the effects of the boundary conditions that affect the transport measurements can be minimized.

An attempt to carry out relative measurements has been done by Liang *et al*. who proved the feasibility of the differential approach to electrically characterize isomeric aromatic molecules using a combination of CT-AFM and density functional theory based Tersoff−Hamann calculations.[19] The authors used an AFM-based nanolithographic technique performed in a liquid environment, referred to as nanografting,[25] to build a nanopatch of one molecule inside the SAM made of its isomer and then electrically characterized the bimolecular system using CT-AFM. The contribution of the different functional groups and of the gold−thiol link to electron tunneling through two distinct monolayers was pointed out. The authors conclude by highlighting the large spread in absolute current values obtained in different experiments but focusing on the fact that the ratios between different molecules are reasonably constant.

The drawback of this differential approach is the impossibility to obtain an absolute measure of the electron transport through a specific type of molecules unless comparing it with one well characterized by absolute measurements. However, if the molecules considered in the same experiment belong to the same family, *e.g.*, alkanethiols, we can obtain quantitative information about specific physical properties that are a function, for instance, of the molecular length or of the arrangement of chemical groups along the chain. An effort to characterize mixed SAMs of alkanethiols of different length using an STM has been reported by Weiss and co-workers[18] introducing a bilayer model to explain their results.

The present paper pushes the differential philosophy to its limit by fabricating at least two patches of different thiols in a simple reference monolayer. The simultaneous presence of these molecules on the surface allows us evaluate directly the ratio between currents. As a test case we apply the technique to the chain length dependence of electron transport in alkanethiol molecules obtaining a value of the electron tunnel decay constant β with unprecedented precision.

RESULTS AND DISCUSSION

Nanofabrication and Measurements. Using nanografting, we fabricate *several* monolayer-thick nanoassemblies of alkanethiols of different chain length, side by side, into a reference alkanethiol SAM on a gold film. M-m-M junctions are then created by placing a clean conducting AFM tip in contact with the top part of the molecules and scanning the surface while a fixed tip–surface bias voltage is applied. The current flowing through the nanografted patches and through the reference monolayer (the carpet) can be recorded in a single image, where differences in contrast are representative of the variation of current levels. Current data coming from all images are then used to determine the average current values for a specific applied bias looking over the current histogram of the image. The force feedback circuit of the AFM controls the mechanical load on the nanocontact keeping it constant while the current image is collected. The current image, together with the topographic image acquired by reading out the AFM laser-deflection feedback, is simultaneously registered. This provides the capability to obtain information about order in the monolayer packing by measuring the patch-to-carpet height difference and comparing this number with the one evalu-

TABLE 1. Patch Height Differences Relative to a C18 Reference SAM[a]

	C18−C8	C18−C9	C18−C10
experimental	1.085 ± 0.027 nm	0.981 ± 0.036 nm	0.869 ± 0.027 nm
theoretical	1.083 ± 0.001 nm	0.974 ± 0.001 nm	0.866 ± 0.001 nm
deviation	0.2%	0.7%	0.3%

[a]The experimental differences are defined as the distance between the centers of the Gaussians describing the height distribution in the topographic images taken around the patch of interest. The theoretical differences are obtained by multiplication of a methylene height contribution (1.082 Å) times the difference in carbon units between the C18 reference SAM and the molecule composing the patch.

ated by assuming that the alkanethiol molecules are inclined by about 30° with respect to the surface normal[26,27] (see Table 1 in Methods). To go one step further, the tip load can be increased to induce controlled changes in the molecular configuration of the SAMs to be correlated with changes in the transport through the M-m-M junction.[28,29] The feasibility of this approach for order evaluation has been proven several times for different applications.[19,25,30–33] The well-defined physical structures resulting from nanografting are ideal for measuring in a comparative way properties such as mechanical stability and electron transfer. In the following we will show that, because of ubiquitous problems with the AFM tip cleanliness, a bilayer junction is needed to model the transport through the M-m-M junction created by using the AFM metal tip as one of the two electrodes and that *relative* measurements between molecules that are not too different are the only ones in which the results can be fully trusted.

We have chosen here a set of alkanethiol molecules with slightly different alkyl chain length, namely, 1-octanethiol ($CH_3(CH_2)_7SH$, briefly C8), 1-nonanethiol ($CH_3(CH_2)_8SH$, briefly C9), 1-decanethiol ($CH_3(CH_2)_9SH$, briefly C10), 1-undecanethiol ($CH_3(CH_2)_{10}SH$, briefly C11), and 1-dodecanethiol ($CH_3(CH_2)_{11}SH$, briefly C12). The calculated difference in film thickness between SAMs of two consecutive chains (*e.g.*, the 10-carbon 1-decanethiol and the 11-carbon 1-undecanethiol) is always about 1.1 Å for an alkyl chain tilt angle of 30°.[27] Within these ordered domains, molecules adopt identical conformations and film structure.

Compared with STM, CT-AFM provides the electrical characterization of a SAM with the simultaneous control of the effective tip–surface distance.[18] In CT-AFM the feedback signal is the cantilever deflection and, even at low load, the tip is in contact with the molecules. In principle, the size of the contact area can be varied by changing the applied load. Loads smaller than 0.5 nN are required to prevent any tip penetration into the SAM. However, it is not possible, even at low load, to prevent the tip from gathering up contaminants adsorbed at the top of the SAM. Such contaminants could be, for example, alkanethiol molecules physisorbed on top of the SAM, which will stick to the metallized tip during the scanning. We think that such contaminant

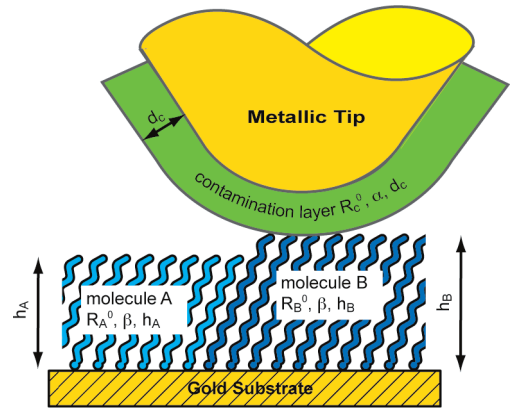

Figure 1. Two-layer tunnel junction model sketching, for example, a nanopatch of short molecules A into a SAM of long ones B. The tip moving from left to right engages two distinct double layers: the contamination layer C and the SAM A, the contamination layer and the SAM B. The two molecular assemblies are characterized by the same contact resistance R^0 and tunnel decay constant β if they fit to the same molecular family (*e.g.*, alkanethiols) but different thickness. Contamination layer properties are usually unknown, but we can make the hypothesis that they stay constant during an image scan on both molecular films. The contact area does not change from A to B since the feedback signal is given by the interaction force.

molecules are responsible for the large fluctuations over the current values observed in previous works.[19] This contamination process is likely to be proportional to the size of the scanning area and to be affected by the surface morphology. In particular we have seen that small area scanning over a very smooth and even area induces very small contamination, while large scan areas on irregular and bumpy regions and, in general, long movement of the tip over the sample, easily change the tip state. In the less perturbative case, *i.e.*, small scanning size and/or smooth surfaces, it is at least reasonable to make the assumption that if a contamination layer covers the tip, such a layer does not change composition and conformation during the entire measurement. Our system will be therefore represented not as a single molecular layer embedded between two electrodes but rather as a more complex double-layer junction.

A tunneling M-m-M junction having two side-by-side SAMs, the nanopatch SAM and the carpet SAM, on the same metal surface is sketched in Figure 1. At the lower level are the molecular assemblies, with a thickness and a conductance determined by the specific molecule; at the upper level is the tip with its contamination layer, which is considered here remaining the same over the whole scanning area. Obviously, each boundary variable influencing electron tunneling through the junction should also be added to the contamination layer.

For testing our differential approach, we have chosen molecules belonging to the alkanethiol family. This enables us to refer to the large volume of experimental and theoretical work that has addressed the chain

length dependence of the electron transfer through alkane σ-bonded bridges. In particular, in the case of alkanethiol SAMs junctions, it has been demonstrated that the electron transport is dominated by coherent nonresonant tunneling and, therefore, the junction resistance depends exponentially on the molecular length[34] and that, for small voltages, the *I*/*V* characteristic is consequently linear.[35] Different kinds of experimental techniques, such as scanning probes,[17,36] metal−molecule−metal junction devices,[37] and electrochemical techniques,[38,39] have shown that the electron current through the junction is proportional to $\exp(-\beta l)$, where β is the tunneling decay constant of the molecules and l is the length of the formed junction. However, the obtained values of β for alkanethiols present in literature widely range from 0.8 to 1.4 $Å^{-1}$ (1.0−1.8 per methylene group).

The resistance of an alkanethiol SAM in a metal−molecule−metal junction as a function of the molecular length is given, under nonresonant conditions, by

$$R = R^0 \exp(\beta h)$$

where the prefactor R^0 is the contact resistance of the SAM, h is the thickness of the SAM, and β is the molecule tunneling decay constant.

In our setup, schematized in Figure 1, we study the transport through two adjacent SAMs of different alkanethiol molecules (referred to as molecules A and B) sandwiched between two metallic contacts. Further, to complete the model description of the junctions, we introduce a third layer that takes into account the presence of contaminants adsorbed on the tip during scanning. The layer is obviously located between the metal AFM tip and the top of the SAM under investigation. Transport through these double junctions is affected by the transmission coefficient of the layers involved (the well-known alkanethiol monolayer and the unknown contamination layer), by the layer-by-layer electron hopping and, clearly, by the contact resistances located at the interface between the metal tip and the contamination layer and between the alkanethiol SAMs and the gold substrate.

Since our resistance depends on an electron tunneling probability, the total resistance of each of the two composite two-layer junctions contains contributions from the SAM and the contamination layer. The system may be described by the relations

$$\begin{cases} R^{A}_{tot} = R^{0}_{tot} V_{CA} \exp(\beta h_A + \alpha d_C) \\ R^{B}_{tot} = R^{0}_{tot} V_{CB} \exp(\beta h_B + \alpha d_C) \end{cases}$$

where the prefactor $R^0{}_{tot}$ is the total contact resistance of all the double junction, the second term is the electron hopping factor linking transport through the two layers, β and α are the tunneling decay constants of the alkanethiol SAMs and of the contamination layer, respectively, h indicates the thickness of the SAMs, and d is the thickness of the contamination layer. A and B indicate the alkanethiol molecules involved while C identifies the contamination layer.

Our model can be further simplified assuming that the alkanethiol molecules, the ones in the surrounding SAM and the ones in the patches, are in the same, unperturbed, standing-up configuration and, as a consequence, that β is the same for both SAMs. Furthermore since all the molecules belong to the same family, it is reasonable to make the hypothesis that the contact resistance at the sulfur−gold interface is the same and that the composition of the contamination layer does not change during repeated tip scans over the two adjacent junctions. As a consequence both α and d_c will stay constant together with the tip/layer contact resistance. Finally, since the two molecules in the SAMs have the same functional end group, we assume that the density of states is the same for both the double junctions.

From all the previous considerations we can easily evaluate the ratio between the total resistances of the two-faced double layers, which simplifies to

$$\frac{R^{A}_{tot}}{R^{B}_{tot}} = \exp(\beta(h_A - h_B))$$

From the last equation, we can extrapolate the value of the decay constant β for the molecules involved:

$$\beta = \frac{\ln\left(\frac{R^{A}_{tot}}{R^{B}_{tot}}\right)}{(h_A - h_B)}$$

Therefore, by measuring point by point in a current image the electron transport through two SAMs of molecules of the same homologous series, placed side-by-side on the same surface, and measuring at the same time their height difference from simultaneously recorded topographic images, as in our approach, we can determine the decay factor β ruling out the effect of the, usually unknown, contact resistance at the tip side of the measurement, as we will demonstrate in the following section.

Direct Differential Comparison of Molecular Systems. We refer hereafter to "differential comparison" between different molecular systems when such comparison is made without the need of any normalization. This is usually possible when all our molecular systems can be imaged, and so characterized, in a single measurement frame, so that we can reasonably assume that the tip does not change during the entire measurement. The ultraflat Ulman gold film, described later on in the methods section, allows for the fabrication of nano-

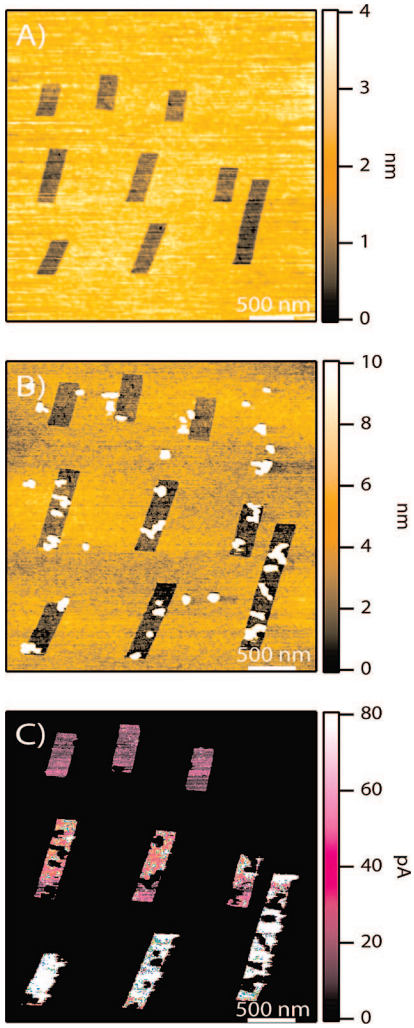

Figure 2. (A) Topographic AFM image acquired with a silicon tip immediately after nanografting of a matrix of 3 × 3 patches containing C10 (first row), C9 (second row), and C8 (third row) molecules embedded in a C18 SAM matrix. Differences in height between the patches and the surrounding C18 SAM are 8.69, 9.81, and 10.85 Å, respectively. (B) Topographic AFM image of the same area acquired with a Pt-coated silicon tip. (C) Current image acquired simultaneously to (B) with the Pt-coated tip at +5.5 mV bias. Distortions in the shape of patches are related to the drift of the *x*−*y* piezo scanner.

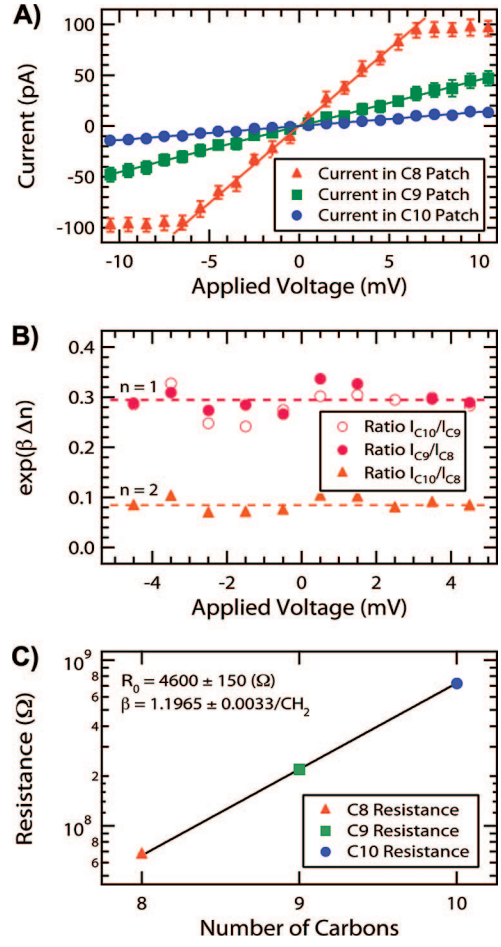

Figure 3. (A) *I*−*V* characteristics of C8, C9, and C10 patches nanografted into a C18 SAM. Flat parts in the C8 plot are due to the saturation of the current amplifier. (B) Current ratios between one-carbon variation chains (C10/C9 and C9/C8) and between two-carbon variation chains (C10/C8). The ratio gives the exponential of the product between the current decay constant and the difference in the number of carbon of the two alkanethiol chains involved. A good overlap of the C10/C9 and C9/C8 ratios is observable. For Δn of 1 and 2, experimental values are very close to the calculated values of 0.301 and 0.091, respectively ($\beta = 1.2/CH_2$). (C) Semilog plot of average resistance *vs* SAM thickness. Fit line is an exponential with β fixed to $1.2/CH_2$.

patches of different molecules close to each other (*e.g.*, in a matrix arrangement). We can therefore acquire the transport information through all the molecules simultaneously in the same image, keeping the size of the same reasonably small.

Figure 2A shows the topographic image of a 3 by 3 matrix of nanopatches, made of three different alkanethiol molecules nanografted into the same C18 SAM background as seen immediately after the nanografting process by a conventional silicon AFM tip. The first row is formed by C10 patches, the second by C9 patches, and the last consists of C8 structures. In this image it is possible to appreciate the flatness of the gold surface, which allows for good height resolution although the scan size is about 3.5 μm by 3.5 μm. Panels B and C of Figure 2 represent the simultaneously acquired topographic and current images recorded after the exchanging of the previous silicon tip with a conductive, Pt covered, one. The current image (Figure 2C) was taken at +5.5 mV bias voltage applied from the surface to the tip. Larger currents flow through the shorter molecule (1-octanethiol), as seen from the color contrast in the figure. Physisorption of dust particles occurs during sample drying as can be seen from the comparison of the two topographic images in panels A and B of Figure 2. Such dust particles generate the no-conduction areas visible inside the patches in Figure 2C. These areas were not taken into account for estimating the current values in the patches. Successively, images of the same area were taken at different applied voltages. Figure 3A shows the average current–voltage (*I*−*V*) trace extrapolated from such images for each

kind of molecule. Every point in the curve is the average from the current values of each patch. The load applied to the tip during scanning was less than 1 nN and the same Pt-coated tip was used for the whole experimental session. All the traces are linear over the voltage sweeps and are used to define a junction resistance equal to 1/slope. Resistances of about 726 ± 15 MΩ, 219 ± 3 MΩ, and 67 ± 1 MΩ were determined for C10, C9, and C8, respectively, with an error of about 2%. The flattening of the current through the C8 patch outside the ±7 mV voltage region is due to the current cutoff due to the saturation of the amplifier.

The ratios between C10/C9, C9/C8, and C10/C8 data are plotted in Figure 3B. These ratios are similar in the cases of C10/C9 and C9/C8, since both differ by one methylene group, and are close to the theoretical value of 0.30. A value of about 0.09 is derived for the ratio between C10 and C8 ($n = 2$). Figure 3C shows a semilog plot of the average junction resistance *versus* alkanethiol chain length for the three molecules involved in the experiment. It is clear that the resistance increases exponentially with the number of methylene groups in the chain, as expected for nonresonant electron tunneling. The slope of the plot gives a tunneling decay constant $\beta = 1.1965 \pm 0.0033$ per methylene group or, ~ 0.94 Å^{-1}, at a contact resistance of about 4600 ± 150 Ω. The C−C length that we used is 1.27 Å.[40] The uncertainty of about 0.3% in the fitting of β leads to an error in the resistance values extrapolated from the plot of about 3.3%.

Normalized Differential Comparison of Molecular Systems. When a direct comparison between SAMs of different alkanethiol molecules is not possible, it becomes crucial to establish a way to compare data coming from different experiments or different frames. In fact, when the tip has to travel longer distances to image all the desired molecular patches, the probability that the tip changes during the measurement increases. What we need then is a correct normalization protocol. In particular, if the hosting SAM is always the same, every molecular patch embedded in it can be referred to that SAM. We refer to this procedure as "normalized differential comparison".

We tested the method using as a substrate a gold film produced by thermal evaporation on hot mica as described in the monolayer preparation section. The final surface was composed of monoatomically flat islands of about 500 nm in diameter. We fabricated nanopatches of C9, C10, and C11 in a matrix of C12 SAM. No more than one patch can be located on the same gold island. Distances between patches of different molecules were about 1 μm. The islands were separated by boundaries that looked as deep as canyons, making it impossible to acquire large images with sufficient height resolution or without current artifacts. For these reasons every patch was imaged separately.

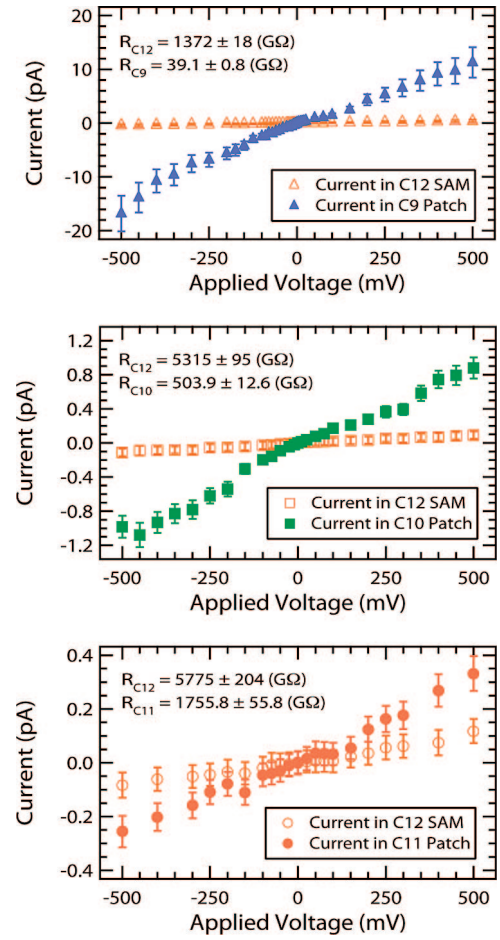

Figure 4. *I*−*V* characteristics of a C9 patch, a C10 patch, and a C11 patch nanografted into a C12 SAM matrix. All the patches were imaged in current independently, which explains the difference in C12 resistance measured in the three cases. Resistance was taken to be the reciprocal of the slope of each straight-line fit. Values for C12 were 1372 ± 18 GΩ, 5315 ± 95 GΩ, and 5775 ± 204 GΩ in the presence of C9, C10, and C11, respectively.

Filled dots in the three plots of Figure 4 represent the *I*−*V* curves for the three measured molecular patches of C9, C10, and C11, respectively, as extrapolated from the set of current images taken at different voltages. Each *I*/*V* curve for each patch is compared, in the same plot, with the *I*/*V* curve determined for the C12 SAM carpet from the same set of images (empty dots in the three plots). Not surprisingly, the three values obtained from the three set of images for the resistance of the C12 SAM are different; in particular we obtained a resistance of 1372 ± 18 GΩ from the C9 patch image, 5315 ± 95 GΩ in the case of the C10 image, and 5775 ± 204 GΩ for the C11 image. It is important to notice here that the resistance is progressively increasing with the number of repeated scans but also that from the first to the last set of images the length of the molecules in the nanopatches increased, both phenomena concurring to the increasing of the contact resistance at the tip. This has an impact also on the measured resistance of the alkanethiol patches, that are 2 or 3 orders

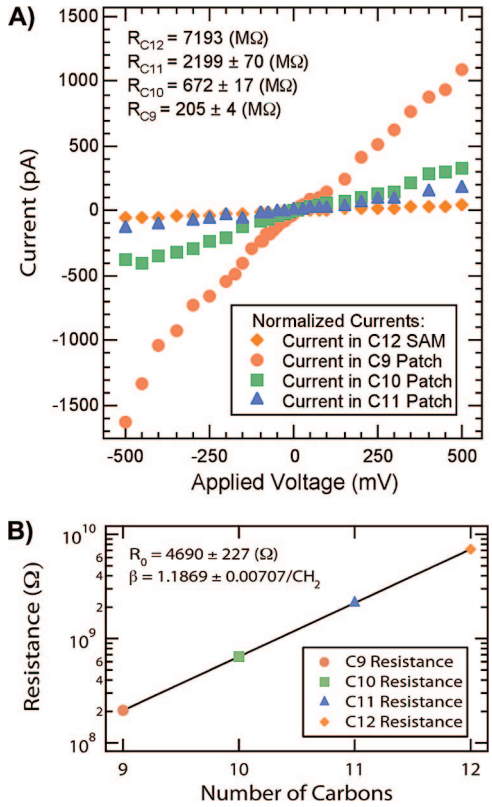

Figure 5. (A) *I*−*V* plot of the normalized C9, C10, and C11 currents. C12 SAM resistance was fixed to the value of about 7193 MΩ, extrapolated extending the plot in Figure 3C to a 12 carbon chain. Ratios between the experimental C12 resistance values and this "theoretical" one were used to normalize all the patches resistances. (B) Semilog plot of normalized resistance *vs* number of carbons constituting the alkanethiol chains. The straight line is an exponential fit done using a contact resistance of about 5 KΩ and decay constant close to 1.187/CH_2. Values are in good agreement with the previous experiment: a difference of 0.8% in the extrapolated values of β for the two experiments gives a difference in calculated resistance values of about 9%.

of magnitude higher with respect to the values expected from the previous section of experiments.

This problem can be overcome by operating a weighted normalization of C9, C10, and C11 resistances. To this end we fix a value for the C12 SAM resistance that is, for simplicity, the value extrapolated from Figure 3C for a 12 carbon chain. Data normalized in this way can be directly compared.

Figure 5A shows the normalized *I*−*V* plots for the four alkanethiol molecules. Filled markers describe the behavior of the molecules in the nanopatches, whereas the empty ones correspond to the 7193 MΩ resistance for C12 SAM extrapolated from the curve in Figure 3C. The normalized data are used to evaluate the resistance of the alkanethiols in term of 1/slope of the *I*−*V* curves. The logarithm of impedance values is then plotted *versus* the number of carbons in the chains (Figure 5B) in order to extrapolate the tunneling current decay constant from the slant of the fitting exponential function. The slope of the plot gives a tunneling decay constant $\beta = 1.1869 \pm 0.0071$/carbon or ~0.93 $Å^{-1}$ at a contact resistance of about 4690 ± 227 Ω. The validity of this differential approach is corroborated by the fact that the β values of the two experiments are very close to one another (less than 1%) meaning that we are not distorting the true physical meaning of the data.

CONCLUSIONS AND OUTLOOK

We demonstrated here that, by combining nanografting with a differential measurement approach, we can determine the resistance of alkanethiol molecules with an higher precision than was possible so far. Our approach has the considerable advantage of circumventing the problem of the contribution of the junction properties to the molecular transport measurements. By accepting the unavoidable presence of a tip-contamination layer on top of the SAM molecules and by considering relative, instead of absolute, measurements, we have demonstrated that the contribution of such layer can be canceled out, provided that experimental data are correctly normalized. In particular, it is necessary that all the nanopatches of the different molecules involved in the study are imaged simultaneously in the same frame or, alternatively, that the patches are imaged separately while each one is embedded in a reference SAM of the same molecule. The tunneling current decay constant β, obtained from our data is in good agreement with the values reported in the literature. Moreover, the determination of *I*/*V* characteristics in our approach is faster and has a much lower experimental error when compared with other point-by-point *I*/*V* methods, due to the high number of data points obtained from a single image.

As shown in Figure 4, the errors affecting current measurements increase as the length of the molecules under investigation increases. An explanation of this trend can be found in the higher resistance of such molecules and, therefore, the low detected currents that force the amplifier to work closely to its sensing limit. Differential comparison between longer molecules is actually under investigation using an improved amplification chain.

Concerning the setup presented in this work, and in particular the experimental environment, there are other complications that have to be addressed. When working in air, in fact, the adhesion effect of atmospheric water has to be taken into account. A perfect knowledge of the force applied by the tip is impossible in air. Measured tip−SAM pull-off forces can reach tens of nanonewtons, depending on tip radius, meaning that even at nominal zero applied force, there is an effective load of up to 15 nN load on the junction. This effect may be controlled moving to a vacuum or a liquid environment. The latter route, even if more challenging, looks like the most promising one, especially when the aim, as in our case, is to extend this kind of study to more complex, biological systems in their physiological environment.

METHODS

Materials and Instrumentation. Gold wire (99.99% pure) was purchased from Metalli Preziosi S.p.a., Milan, Italy, Muscovite mica from Goodfellow Cambridge Limited, Huntingdon, England. Ethanol (99.8% purity), and all alkanethiols were used as received from Fluka and Sigma Aldrich. All the measurements were carried out using a commercial NT-MDT Solver PRO AFM endowed with a low-noise, high-gain amplifier (AU020-NTF, NT-MDT Co.) characterized by a 3 fA $Hz^{-1/2}$ noise level, and able to measure currents up to 100 pA, where the amplifier saturates. Nanografting was performed in an open liquid cell using silicon rectangular cantilevers (μmash NSC36/noAl, spring constant 0.6 nN/nm) while all the current measurements were carried out with conductive Pt covered silicon V-shaped cantilevers (μmash CSC21/TiPt, spring constant 0.12 nN/nm). The loads applied during imaging and current measurements were set to about 0.5 nN in order to ensure good tip−film contact avoiding at the same time penetration of the monolayer. In the case of nanografting, the load was as large as 50 nN. Current measurements were carried out under atmospheric conditions.

Monolayer Preparation. Two different kinds of gold substrates were used in the described experiments: a cold deposited gold surface obtained by slightly revising the procedure described by the Ulman group in ref (referred to as Ulman gold) and a hot deposited gold on mica.

Briefly, a thin gold film was first thermally deposited onto a freshly cleaved mica surface that afterward was cut into 8 × 8 mm^2 pieces. Epoxy SU8-100 glue was then distributed in drops on the gold side of the slides. The samples were backed at 95 °C for 5 h in order to remove the solvent from the glue drops. Successively the SU8 was cured by exposure under a 462 nm wavelength UV lamp at a power of about 70 $\mu W/cm^2$ for 15 min. All samples were then annealed at 95 °C for at least 3 h. The SU8 drop, now looking as a flat hard surface strongly attached to the gold layer, can in this way be mechanically detached in air from the mica substrate, keeping the gold film attached to it. The surface of gold originally buried at the interface with the mica is now available. Such a Au film surface has the advantage of reproducing the flatness of mica, giving an extremely reduced roughness of about 4 Å. Gold island boundaries look very light and almost indistinguishable from large-scale topographic images. Samples are, immediately after stripping, soaked in a freshly prepared 100 μm solution of thiols in ethanol.

The second kind of substrate used in the present work is a more conventional gold film deposited onto heated mica substrates using a thermal evaporator at a background pressure of 5×10^{-8} Torr. Freshly cleaved mica was inserted into the vacuum chamber and subsequently backed at 400 °C for 24 h. Typically, 800 Å of gold was deposited at 0.2 Å/s with the substrate heated at a temperature of about 340 °C. Immediately after metallization and cooling down to room temperature, the gold was placed into freshly prepared 100 μm thiol solution in ethanol for at least 48 h.[42]

Before use, each sample was rinsed with several milliliters of absolute ethanol and gently blown dry with nitrogen.

Junction Formation and Characterization. Our junctions are formed by nanopatches of the molecules of interest inlaid in a reference SAM matrix. The molecular patches or the surrounding SAM are then "sandwiched" between the supporting gold surface and a platinum-covered AFM tip that acts as the second metallic contact of the junction.

For the nanofabrication we start from a gold surface with a well-packed SAM on top of it. The whole procedure is performed in a sealed liquid cell filled with an ethanol solution (100 μm) of a different thiolated molecule. SAM molecules are easily imaged by AFM by using a low imaging force of about 0.5 nN. If we increase the force above a certain threshold, which depends on the molecule's chain length, the molecules of the SAM are displaced during the scan and replaced by the ones in solution which self-assemble on the freshly exposed gold surface. In the case of alkanethiol molecules, using a tip with a radius smaller than 10 nm, the threshold is around 50 nN. The resulting nanofeatures, of about 200 × 200 nm^2, can be imaged by AFM at low imaging force, *e.g.*, 0.5 nN. The molecules in the patch rapidly self-assemble, due to the nanometer-confined environment and to the tip local effect.[31] Completion of the molecular substitution can be proved by resolving the (✓3 × ✓3)R30° structure of alkanethiols on Au(111) film inside the patch[30] or from the height distribution analysis. Table 1 reports the measured height differences between C8, C9, and C10 nanopatches and a surrounding C18 reference SAM. Each value has been obtained by measuring the distance between the Gaussians describing the height distribution of the patch and of the SAM molecules in a sufficiently large area holding the patch of interest. Theoretical values are also reported as comparison. The height differences between C8 and C9 and between C9 and C10 (corresponding of a single methylene group height contribution) are about 0.104 and 0.112 nm, respectively, both very close to the theoretical value of about 0.11 nm.[18]

After nanografting, the silicon tip is removed and replaced with a Pt-covered conductive one. Tip replacement is always necessary after nanografting, because this process degrades the tip reducing its sharpness and generally contaminating it. To find the nanostructured area after tip exchanging, we produce on the surface, before nanografting, micrometer-sized markers, easily visible with an optical microscope. The shape of the markers was chosen in order to optimize the repositioning of the AFM tip: with the new tip optically aligned over the markers, the patches are found within a radius of 3 μm or less.

Voltages are then applied between the tip and the substrate, monitoring the current flowing through the molecular assembly. The force applied by the tip was, at all times, less than 0.5 nN in order to ensure good electrical coupling, avoiding at the same time tip penetration into the SAM. In fact, above 1 nN, a lower value for the height difference between the patch and the SAM was measured.[32] The range of voltage sweep during current measurements was indirectly limited by the maximum value of current readable by the amplifier, that is ±100 pA. In any case, in order to avoid damaging of the layers, voltages larger than ±500 mV were never used in the experiments. Scanning speed during current imaging was always below 200 nm/s.

From current images, collected at different applied voltages, we have extrapolated the values of current flowing through each type of molecule present on the surface. Currents are defined as the mean value of the Gaussians describing the current distribution over the patches and, eventually, over the surrounding reference SAM. This procedure is repeated for each patch and obtained values are successively used to draw the *I*−*V* characteristic for every molecule as shown in Figure 3. We would like to point out here that a single current image contains a large amount of data (usually 512 × 512 sampled pixels) and therefore statistical information on the molecular conductance. As a result, the electrical characterization of a group of molecules can be obtained from the analysis of few tens of current images, one for each voltage value, instead of the thousands of *I*/*V* curves needed in the case of single-point measurements.

Acknowledgment. This research has been partially supported by MIUR through PRIN. The authors gratefully acknowledge Sandro Scandolo, Silvano De Franceschi, Marco Lazzarino, and Jian Liang for helpful discussions.

REFERENCES AND NOTES

1. Guiducci, C.; Stagni, C.; Zuccheri, G.; Bogliolo, A.; Benini, L.; Samorì, B.; Riccò, B. DNA Detection by Integrable Electronics. *Biosens. Bioelectron.* **2004**, *19*, 781–787.
2. Fritz, J.; Cooper, E. B.; Gaudet, S.; Sorger, P. K.; Manalis, S. R. Electronic Detection of DNA by Its Intrinsic Molecular Charge. *Proc. Natl. Acad. Sci. U.S.A.* **2002**, *99*, 14142–14146.
3. Pourmand, N.; Karhanek, M.; Persson, H. H.; Webb, C. D.; Lee, T. H.; Zahradníková, A.; Davis, R. V. Direct Electrical Detection of DNA Synthesis. *Proc. Natl. Acad. Sci. U.S.A.* **2006**, *103*, 6466–6470.
4. Chang, T.; Tsai, C.; Sun, C.; Chen, C.; Kuo, L.; Chen, P. Ultrasensitive Electrical Detection of Protein Using Nanogap Electrodes and Nanoparticle-Based DNA Amplification. *Biosens. Bioelecton.* **2007**, *22*, 3139–3145.

5. Bandiera, L.; Cellere, G.; Cagnin, S.; De Toni, A.; Zanoni, E.; Lanfranchi, G.; Lorenzelli, L. A Fully Electronic Sensor for the Measurement of cDNA Hybridization Kinetics. *Biosens. Bioelectron.* **2007**, *22*, 2108–2114.
6. Ghosh, A. W.; Damle, P. S.; Datta, S.; Nitzan, A. Molecular Electronics: Theory and Device Prospects. *MRS Bull.* **2004**, *29*, 391–395.
7. Salomon, A.; Cahen, D.; Lindsay, S.; Tomfohr, J.; Engelkes, V. B.; Frisbie, C. D. Comparison of Electronic Transport Measurements on Organic Molecules. *Adv. Mater.* **2003**, *15*, 1881–1890.
8. Zhou, C.; Deshpande, M. R.; Reed, M. A.; Jones II, L.; Tour, J. M. Nanoscale Metal/Self-Assembled Monolayer/Metal Heterostructures. *Appl. Phys. Lett.* **1997**, *71*, 611–613.
9. Wang, W.; Lee, T.; Reed, M. A. Elastic and Inelastic Electron Tunneling in Alkane Self-Assembled Monolayers. *J. Phys. Chem. B* **2004**, *108*, 18398–18407.
10. Selzer, Y.; Salomon, A.; Cahen, D. Effect of Molecule-Metal Electronic Coupling on Through-Bond Hole Tunneling across Metal-Organic Monolayer-Semiconductor Junctions. *J. Am. Chem. Soc.* **2002**, *124*, 2886–2887.
11. Rampi, M. A.; Schueller, O. J.; Whitesides, G. M. Alkanethiol Self-Assembled Monolayers as the Dielectric of Capacitors With Nanoscale Thickness. *Appl. Phys. Lett.* **1998**, *72*, 1781–1783.
12. Reed, M. A.; Zhou, C.; Muller, C. J.; Burgin, T. J.; Tour, J. M. Conductance of a Molecular Junction. *Science* **1997**, *278*, 252–254.
13. Xu, B.; Tao, N. J. Measurement of Single-Molecule Resistance by Repeated Formation of Molecular Junctions. *Science* **2003**, *301*, 1221–1223.
14. He, J.; Sankey, O.; Lee, M.; Tao, N.; Li, X.; Lindsay, S. Measuring Single Molecule Conductance With Break Junctions. *Faraday Discuss.* **2006**, *131*, 145–154.
15. Tans, S. J.; Verschueren, A. R.; Dekker, C. Room-Temperature Transistor Based on a Single Carbon Nanotube. *Nature* **1998**, *393*, 49–52.
16. Metzger, R. M. Electrical Rectification by a Molecule: The Advent of Unimolecular Electronic Devices. *Acc. Chem. Res.* **1999**, *32*, 950–957.
17. Wold, D. J.; Frisbie, C. D. Formation of Metal-Molecule-Metal Tunnel Junctions: Microcontacts to Alkanethiol Monolayers with a Conducting AFM Tip. *J. Am. Chem. Soc.* **2000**, *122*, 2970–2971.
18. Bumm, L. A.; Arnold, J. J.; Dunbar, T. D.; Allara, D. L.; Weiss, P. S. Electron Transfer through Organic Molecules. *J. Phys. Chem. B* **1999**, *103*, 8122–8127.
19. Liang, J.; Sun, Q.; Selloni, A.; Scoles, G. Side-by-Side Characterization of Electron Tunneling through Monolayers of Isomeric Molecules: A Combined Experimental and Theoretical Study. *J. Phys. Chem. B* **2006**, *110*, 24797–24801.
20. Cui, X. D.; Primak, A.; Zarate, X.; Tomfohr, J.; Sankey, O. F.; Moore, A. L.; Moore, T. A.; Gust, D.; Harris, G.; Lindsay, S. M. Reproducible Measurement of Single-Molecule Conductivity. *Science* **2001**, *294*, 571–574.
21. Magoga, M.; Joachim, C. Conductance of Molecular Wires Connected or Bonded in Parallel. *Phys. Rev. B* **1999**, *59*, 16011–16021.
22. Onipko, A. Analytical Model of Molecular Wire Performance: A Comparison of π and σ Electron Systems. *Phys. Rev. B* **1999**, *59*, 9995–10006.
23. Datta, S.; Tian, W.; Hong, S.; Reifenberger, R.; Henderson, J. I.; Kubiak, C. P. Current-Voltage Characteristics of Self-Assembled Monolayers by Scanning Tunneling Microscopy. *Phys. Rev. Lett.* **1997**, *79*, 2530–2533.
24. Gonzalez, C.; Simòn-Manso, Y.; Batteas, J.; Marquez, M.; Ratner, M.; Mujica, V. A Quasimolecular Approach to the Conductance of Molecule-Metal Junctions: Theory and Application to Voltage-Induced Conductance Switching. *J. Phys. Chem. B* **2004**, *108*, 18414–18420.
25. Amro, N. A.; Xu, S.; Liu, G.-Y. Patterning Surfaces Using Tip-Directed Displacement and Self-Assembly. *Langmuir* **2000**, *16*, 3006–3009.
26. Poirier, G. E. Characterization of Organosulfur Molecular Monolayers on Au(111) using Scanning Tunneling Microscopy. *Chem. Rev.* **1997**, *97*, 1117–1127.
27. Bumm, L. A.; Arnold, J. J.; Charles, L. F.; Dunbar, T. D.; Allara, D. L.; Weiss, P. S. Directed Self-Assembly to Create Molecular Terraces with Molecularly Sharp Boundaries in Organic Monolayers. *J. Am. Chem. Soc.* **1999**, *121*, 8017–8021.
28. Barrena, E.; Ocal, C. Molecular Macking Changes of Alkanethiols Monolayers on Au(111) Under Applied Pressure. *J. Chem. Phys.* **2000**, *113*, 2414–2418.
29. Song, H.; Lee, H.; Lee, T. Intermolecular Chain-to-Chain Tunneling in Metal-Alkanethiol-Metal Junctions. *J. Am. Chem. Soc.* **2007**, *129*, 3806–3807.
30. Xu, S.; Liu, G.-Y. Nanometer-Scale Fabrication by Simultaneous Nanoshaving and Molecular Self-Assembly. *Langmuir* **1997**, *13*, 127–129.
31. Xu, S.; Miller, S.; Laibinis, P. E.; Liu, G.-Y. Fabrication of Nanometer Scale Patterns within Self-Assembled Monolayers by Nanografting. *Langmuir* **1999**, *15*, 7244–7251.
32. Castronovo, M.; Bano, F.; Raugei, S.; Scaini, D.; Dell'Angela, M.; Hudej, R.; Casalis, L.; Scoles, G. Mechanical Stabilization Effect of Water on a Membrane-like System. *J. Am. Chem. Soc.* **2007**, *129*, 2636–2641.
33. Liu, G.-Y.; Xu, S.; Qian, Y. Nanofabrication of Self-Assembled Monolayers Using Scanning Probe Lithography. *Acc. Chem. Res.* **2000**, *33*, 457–466.
34. Wold, D. J.; Frisbie, C. D. Fabrication and Characterization of Metal-Molecule-Metal Junctions by Conducting Probe Atomic Force Microscopy. *J. Am. Chem. Soc.* **2001**, *123*, 5549–5556.
35. Simmons, J. G. Generalized Formula for the Electric Tunnel Effect between Similar Electrodes Separated by a Thin Insulating Film. *J. Appl. Phys.* **1963**, *34*, 1793–1803.
36. Salmeron, M.; Neubauer, G.; Folch, A.; Tomitori, M.; Ogletree, D. F.; Sautet, P. Viscoelastic and Electrical Properties of Self-Assembled Monolayers on Au(111) Films. *Langmuir* **1993**, *9*, 3600–3611.
37. Wang, W.; Lee, T.; Reed, M. A. Mechanism of Electron Conduction in Self-Assembled Alkanethiol Monolayer Devices. *Phys. Rev. B* **2003**, *68*, 035416.
38. Chidsey, C. Free Energy and Temperature Dependence of Electron Transfer at the Metal-Electrolyte Interface. *Science* **1991**, *251*, 919–922.
39. Sachs, S.; Dudek, S.; Hsung, R.; Sita, L.; Smalley, J.; Newton, M.; Feldberg, S.; Chidsey, C. Rates of Interfacial Electron Transfer through π-Conjugated Spacers. *J. Am. Chem. Soc.* **1997**, *119*, 10563–10564.
40. Israelachvili, J. N. *Intermolecular & Surface Forces*; Academic Press Limited: London, 1991; pp 88–89..
41. Gupta, P.; Loos, K.; Korniakov, A.; Spagnoli, C.; Cowman, M.; Ulman, A. Facile Route to Ultraflat SAM-Protected Gold Surfaces by "Amphiphile Splitting". *Angew. Chem., Int. Ed.* **2004**, *43*, 520–523.
42. Ulman, A. Formation and Structure of Self-Assembled Monolayers. *Chem. Rev.* **1996**, *96*, 1533–1554.